Journal of Materials Chemistry A

PAPER

View Article Online
View Journal | View Issue

Cite this: J. Mater. Chem. A, 2017, 5, 24371

A stable two-electron-donating phenothiazine for application in nonaqueous redox flow batteries†

Jeffrey A. Kowalski, ‡[ab] Matthew D. Casselman, ‡[c] Aman Preet Kaur,[c] Jarrod D. Milshtein, [ad] Corrine F. Elliott, [c] Subrahmanyam Modekrutti,[c] N. Harsha Attanayake,[c] Naijao Zhang,[c] Sean R. Parkin, [c] Chad Risko, [ce] Fikile R. Brushett *[ab] and Susan A. Odom *[c]

Received 6th July 2017
Accepted 24th October 2017

DOI: 10.1039/c7ta05883g

rsc.li/materials-a

Stable electron-donating organic compounds are of interest for numerous applications that require reversible electron-transfer reactions. Although many organic compounds are stable one-electron donors, removing a second electron from a small molecule to form its dication usually leads to rapid decomposition. For cost-effective electrochemical energy storage utilizing organic charge-storage species, the creation of high-capacity materials requires stabilizing more charge whilst keeping molecular weights low. Here we report the simple modification of *N*-ethylphenothiazine, which is only stable as a radical cation (not as a dication), and demonstrate that introducing electron-donating methoxy groups *para* to nitrogen leads to dramatically improved stability of the doubly oxidized (dication) state. Our results reveal that this derivative is more stable than an analogous compound with substituents that do not allow for further charge delocalization, rendering it a promising scaffold for developing atom-efficient, two-electron donors.

Introduction

Electrochemical energy storage is expected to play a critical role in meeting the electric power sector's emerging needs by facilitating the integration of intermittent renewable resources and by enhancing the efficiency of non-renewable energy processes.[1,2] Redox flow batteries (RFBs) are well suited for multi-hour, rechargeable energy storage, and offer several key advantages over enclosed battery technologies (*e.g.*, lithium (Li)-ion, lead-acid), including independent scaling of power and energy, long service life, improved thermal and chemical management, and simplified manufacturing.[3,4] However, state-of-the-art RFB systems have yet to achieve widespread commercial success due to technical and economic challenges,[5] which, in turn, have spurred research into alternative chemistries with improved properties.

Organic redox couples have emerged as an attractive alternative to traditional transition metal salts.[6,7] Organic materials are particularly appealing for RFB applications because their electrochemical and physical properties can be tuned through functionalization, thereby expanding the molecular design space. Moreover, several classes of organic compounds undergo reversible two-electron redox processes,[8–10] doubling the charge-storage capacity relative to electrolytes containing the same concentration of a single electron transfer redox-active material. Although many organic redox couples have been proposed and a few systems have been characterized,[11–28] systematic structure–function studies have been limited, likely due to the challenges associated with synthesis and electrochemical characterization of these materials, as well as the relative novelty of the field.

Phenothiazines provide a promising and scalable platform for the development of electron-donating materials. Indeed, derivatization of phenothiazine has afforded numerous products in the pharmaceutical industry (*e.g.*, methylene blue, promethazine, and chlorpromazine).[29–31] The general stability of phenothiazine derivatives in the radical-cation form has enabled their incorporation as one-electron donors in a variety of electronic and electrochemical devices including photo-redox catalysts in atom-transfer radical polymerizations,[32,33] active materials in electrochromic displays,[34,35] semiconductors in organic field-effect transistors,[36] and redox shuttles in dye-sensitized solar cells.[37] In the field of electrochemical energy storage, phenothiazines have been reported as redox shuttles to protect against cell overcharge and subsequent thermal

[a]Joint Center for Energy Storage Research, USA
[b]Department of Chemical Engineering, Massachusetts Institute of Technology, Cambridge, MA 02139, USA. E-mail: brushett@mit.edu
[c]Department of Chemistry, University of Kentucky, Lexington, KY 40506, USA. E-mail: susan.odom@uky.edu
[d]Department of Materials Science and Engineering, Massachusetts Institute of Technology, Cambridge, MA, 02139, USA
[e]Center for Applied Energy Research, University of Kentucky, Lexington, KY 40511, USA

† Electronic supplementary information (ESI) available: Synthetic procedures, NMR spectra, X-ray crystal structures, cyclic voltammetry, bulk electrolysis. CCDC 1480992. For ESI and crystallographic data in CIF or other electronic format see DOI: 10.1039/c7ta05883g

‡ These authors contributed equally to the work.

runaway in Li-ion batteries. Notably, Dahn and co-workers demonstrated extensive overcharge protection of Li-ion cells using *N*-alkylated phenothiazines as redox shuttles.[38,39] More recently, we have reported effective overcharge mitigation at higher voltages, enabled by molecular functionalization of the phenothiazine core.[40–42]

Given these properties, phenothiazines hold considerable promise for RFB applications. *N*-(2-Methoxyethyl)phenothiazine (MEPT) and *N*-(2-(2-methoxyethoxy)ethyl)phenothiazine (MEEPT)[43] are highly miscible in nonaqueous electrolytes, and their radical cations are sufficiently stable to permit their isolation as crystalline salts. Their stability is further demonstrated by cycling symmetric flow cells containing 0.5 M active material. At constant current densities as high as 100 mA cm^{-2}, capacity fade was undetectable after 100 deep charge/discharge cycles (experimental runtime of over 80 h).[43]

Although the radical cations of MEPT and MEEPT are stable in a variety of nonaqueous electrolytes, their dication states are subject to rapid decomposition, limiting their capacity to one redox event per molecule. To increase the capacity of phenothiazines for use as active materials in RFBs, we explored derivatization at positions on the periphery of the conjugated ring system, specifically targeting the reactive positions *para* to nitrogen (3 and 7). A variety of derivatives containing substituents at the 3 and 7 positions undergo an irreversible second oxidation event, as determined by cyclic voltammetry (CV) experiments. However, substituents that are both electron-donating and conjugated could result in extended charge delocalization that may stabilize the dication state. Here, we report the synthesis and characterization of a phenothiazine derivative containing conjugated electron-donating substituents, *N*-ethyl-3,7-dimethoxyphenothiazine (DMeOEPT, Fig. 1). For comparison, we examined the performance of parent compound *N*-ethylphenothiazine (EPT, Fig. 1) and a derivative containing electron-donating methyl substituents at the 3 and 7 positions (DMeEPT, Fig. 1) in which charge delocalization is expected to be less extensive compared to DMeOEPT.

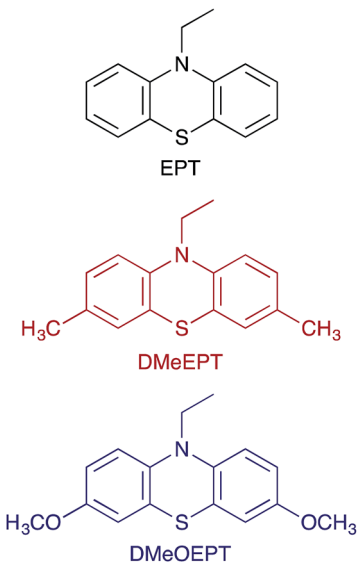

Fig. 1 Representations of the chemical structures of *N*-ethylphenothiazine (EPT, black, top), *N*-ethyl-3,7-dimethylphenothiazine (DMeEPT, red, middle), and *N*-ethyl-3,7-dimethoxyphenothiazine (DMeOEPT, blue, bottom).

Results and discussion

EPT[44] and DMeEPT[40] were synthesized as previously reported. The synthesis of DMeOEPT was accomplished in two high-yielding steps from EPT. Bromination of EPT with *N*-bromosuccinimide gave previously reported 3,7-dibromo-*N*-ethylphenothiazine (DBrEPT).[40] Subsequent methoxylation was accomplished using sodium methoxide/copper(I) iodide. In addition to analysis by nuclear magnetic resonance spectroscopy (Fig. S1 and S2†) and mass spectrometry, X-ray analysis of single crystals grown in methanol/water (Fig. S3†) confirms the structure of the product. Atom economy is an important factor for charge storage.[5] At 287 g mol^{-1}, the molecular weight of DMeOEPT is 60 g mol^{-1} greater than EPT (227 g mol^{-1}), constituting an approximate 26% increase in molecular weight. However, if DMeOEPT's doubly oxidized form is stable, an increase of 58% in overall molecular gravimetric capacity could be achieved as compared to parent EPT, which can reversibly donate only one electron.

Cyclic voltammograms of EPT, DMeEPT, and DMeOEPT in propylene carbonate (PC) containing 1 M lithium bis(trifluoromethane)sulfonimide (LiTFSI) are shown in Fig. 2. The voltammograms depict electrochemically reversible first oxidation events and the formation of stable radical cations, as evidenced by peak-potential separations of 60–62 mV and peak-current ratios near 1, with all values independent of scan rate (Fig. S15†). The first oxidation event proceeds most readily for DMeOEPT (0.068 V *vs.* ferrocenium/ferrocene ($Cp_2Fe^{+/0}$)), followed by DMeEPT (0.174 V *vs.* $Cp_2Fe^{+/0}$), and then EPT (0.289 V *vs.* $Cp_2Fe^{+/0}$). This trend is consistent with the Hammett constants of the substituents: methoxy (−0.27) donates more strongly than methyl (−0.17), which, in turn, donates more strongly than hydrogen (0.0).[45] With EPT and DMeEPT, the second oxidation event is less reversible, as shown by peak separations significantly larger than 60 mV and peak-current ratios greater than 1. While these characteristics suggest the formation of unstable dications in both cases, the peak symmetries are consistent with DMeEPT having a more stable dication than EPT. By contrast, the second oxidation event of DMeOEPT is reversible, with a peak separation of 60 mV and a peak-current ratio of 1.02 ± 0.03, again independent of the scan rate, demonstrating that the DMeOEPT dication is stable on the cyclic voltammetry experimental timescale (*ca.* 12–120 s). DMeOEPT exhibits similar behavior in 1 M $LiBF_4$ in PC and 1 M $TBAPF_6$ in acetonitrile (Fig. S26†), indicating that the second electron transfer is stable in both electrolytes. While the oxidation potentials of DMeOEPT are lower by about 200–300 mV compared to EPT, the ability to access both electron transfer events increases the net potential of this donor. The average potential of the two redox events for DMeOEPT, at *ca.* 0.350 V *vs.* $Cp_2Fe^{+/0}$, which is about 60 mV higher than the first oxidation potential of EPT at 0.289 V *vs.* $Cp_2Fe^{+/0}$. In general,

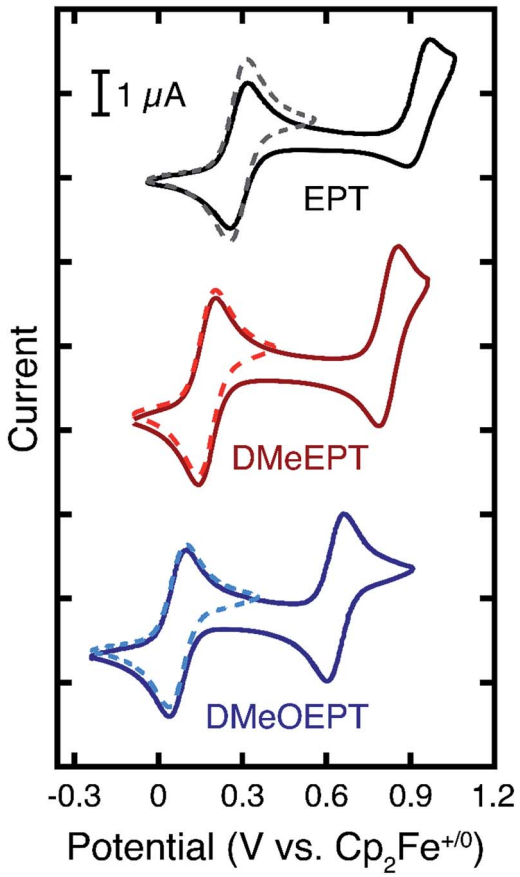

Fig. 2 Cyclic voltammograms of the first and second oxidations of 1 mM EPT (black, top), DMeEPT (red, middle), and DMeOEPT (blue, bottom) in 1 M LiTFSI in PC at a scan rate of 10 mV s^{-1}. Solid lines depict CVs accessing both oxidation reactions, while dashed lines depict CVs accessing the first oxidation alone.

this tradeoff highlights a key challenge in molecular engineering of active species; specifically, attempting to enhance one property (*e.g.* molecular charge capacity) can often have unintended negative effects on other desirable properties (*e.g.* redox potential). Understanding and controlling these tradeoffs is necessary for designing active species with property sets that align with a desired application.

Diffusion coefficients were estimated by applying the Randles–Sevcik equation to the positive sweep of the CV for the neutral species and the negative sweep of the CV for the radical-cation salts at various scan rates (Fig. S15†). As expected, the diffusion coefficient decreases with increasing molecular size. Additionally, the diffusion coefficient for the radical cation of each species is lower than that of the corresponding neutral species, likely due to interactions with counter-ions in solution, which contribute to a larger effective radius.§ Finally, the relative solubilities of EPT, DMeEPT, and DMeOEPT were measured

§ We note that the response for the radical-cation salt may be complicated by the presence of two anions (BF_4^- from the synthesis and $TFSI^-$ from the supporting salt); however, we do not expect a dramatic change in the apparent diffusion coefficient because of the thousand-fold difference in concentration between the BF_4 anions (1 mM) and the TFSI anions (1 M).

Table 1 Measured half-wave potentials, peak separations, and peak-current ratios for the first and second oxidations, diffusion coefficients, and solubilities of EPT, DMeEPT, and DMeOEPT, their tetrafluoroborate radical-cation salts, and their tetrafluoroborate dication salts in 1 M LiTFSI in PC. For clarity, the radical-cation values are italicized and the dication is bolded. All cyclic voltammetry was performed at 1 mM active material concentration. The peak separations and peak-current ratios were calculated at a scan rate of 10 mV s^{-1}

	First oxidation			Second oxidation				
Compound	Potential (V *vs.* $Cp_2Fe^{+/0}$)	Peak separation (mV)	Peak current ratio ($i_{p,ox}/i_{p,red}$)	Potential (V *vs.* $Cp_2Fe^{+/0}$)	Peak separation (mV)	Peak current ratio ($i_{p,ox}/i_{p,red}$)	Diffusion coefficient—neutral, radical cation ($\times 10^{-6}$ cm^2 s^{-1})	Compound solubility neutral, radical cation, dication (M)
EPT	0.289 ± 0.001	60 ± 1	1.007 ± 0.001	0.928 ± 0.001	73 ± 1	14 ± 5	1.7 ± 0.3 *1.3 ± 0.1*	0.10 ± 0.01 *0.42 ± 0.01* —
DMeEPT	0.174 ± 0.001	62 ± 1	1.05 ± 0.01	0.824 ± 0.001	71 ± 2	1.31 ± 0.03	1.3 ± 0.1 *0.9 ± 0.1*	0.07 ± 0.01 *0.12 ± 0.01* —
DMeOEPT	0.068 ± 0.001	60 ± 1	1.01 ± 0.01	0.632 ± 0.001	60 ± 1	1.02 ± 0.03	1.2 ± 0.1 *0.9 ± 0.1*	0.05 ± 0.01 *0.15 ± 0.01* **0.10 ± 0.01**

in the electrolyte. DMeOEPT in LiTFSI/PC has the lowest solubility of the three compounds examined. For all three compounds, the radical cation is more soluble than the neutral species, likely due to the polarity of the electrolyte that results from the high concentration of LiTFSI. All results discussed above are summarized in Table 1.

Spectroelectrochemistry was employed to further investigate the redox processes of EPT, DMeEPT, and DMeOEPT. Dilute solutions of each neutral phenothiazine derivative were prepared in 0.1 M LiTFSI/PC and placed in a spectroelectrochemical cell, which was used to charge the solution. Spectra of each species are shown in Fig. 3, while complete charging and discharging spectra are shown in Fig. S4–S9.† The absorption spectra of the neutral species exhibit absorption onsets and lowest-energy maxima at similar values (EPT at 311 nm, DMeEPT at 314 nm, DMeOEPT at 315 nm). Upon charging, however, significant variations arise. While the lower-energy features are similar for the radical cations of EPT and DMeEPT, with each maximum absorbance at 510–550 nm, the radical cation of DMeOEPT exhibits a more intense, red-shifted absorption feature at 616 nm. The differences among the dication absorption spectra are even more distinctive. The dication of DMeOEPT displays a characteristic maximum that is blue-shifted by about 20 nm relative to its radical-cation form. This feature is significantly more intense than any feature observed in the UV-visible region for either of the EPT or DMeEPT dications. These results demonstrate that the radical cation and dication of DMeOEPT differ in character from the corresponding forms of EPT and DMeEPT, likely due to greater electronic delocalization onto the methoxy groups compared to the hydrogen atoms in EPT or the methyl groups in DMeEPT.

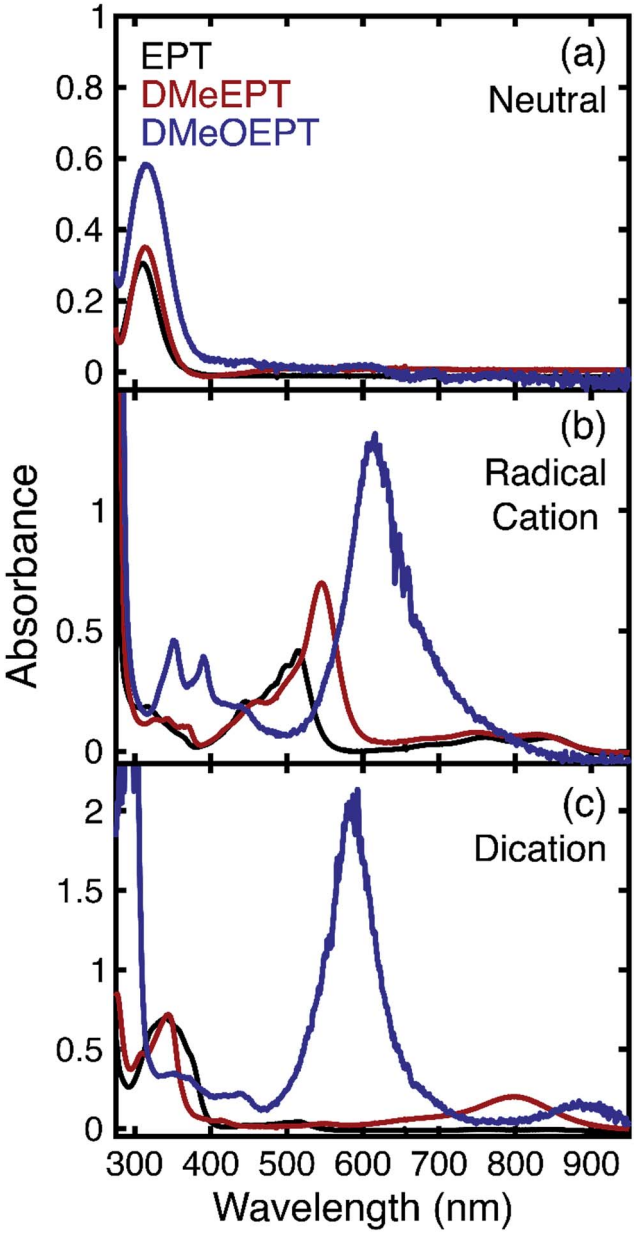

Fig. 3 UV-vis spectra of the neutral (a), radical cation (b), and dication (c) of EPT (black), DMeEPT (red), and DMeOEPT (blue) in 0.1 M LiTFSI in PC. The radical cation and dication were generated by bulk electrolysis of solutions consisting of 0.375 mM active material in 0.1 M LiTFSI/PC.

Density functional theory (DFT) calculations were employed to confirm this hypothesis and, in particular, to evaluate whether the methoxy groups would lead to a larger degree of charge delocalization in the dication state of DMeOEPT, thereby impacting its oxidation potentials and overall chemical stability when compared to EPT and DMeEPT.[46,47] The frontier molecular orbitals for the dication states (highest occupied molecular orbital, HOMO; note that this is the HOMO-1 of the neutral species), determined at the UB3LYP/6-311G(d,p) level of theory, exhibit a greater degree of wavefunction delocalization for DMeOEPT as compared to EPT and DMeEPT (Fig. 4 and S10–S12†). Specifically, the π-based wavefunctions extend onto the methoxy oxygens in DMeOEPT. Mulliken charges were used to provide a numerical representation of the charge delocalization in each system (Table S1†). In DMeOEPT, the methoxy groups hold a greater positive charge in the dication state than do the hydrogen atoms in EPT or methyl groups in DMeEPT, occupying the same positions (per *para* substituent: methoxy +0.30, methyl +0.20, hydrogen +0.20) (Fig. 4). The molecular length of DMeOEPT (13.8 Å in dication form) is larger than EPT (9.4 Å) and DMeEPT (11.4 Å), allowing for electron density of the DMeOEPT dication to be delocalized over a larger volume and over more atoms (Table S2†).

Bulk electrolysis was used to determine the long-term stability of EPT, DMeEPT, and DMeOEPT. Fig. 5 shows the cycling profiles for each of the bulk electrolysis experiments. Fig. 6 compiles the charging capacities across all cycling. First, to validate the technique, EPT was cycled through its first oxidation event, which was shown to be reversible on the CV timescale. Charging to 0.6 V *vs.* $Cp_2Fe^{+/0}$ is sufficient to access the first oxidation event without accessing the second, irreversible event. The coulombic efficiency in this cycling experiment ranged from 99 to 100%, with an overall capacity retention of 96% after 50 charge/discharge cycles at an applied current of 0.804 mA, which should afford a complete charge in 1 hour (Fig. 6 and S16†). The slight capacity fade observed is likely due, at least in part, to species crossover through the porous frit that separates the counter-electrode chamber from the working-

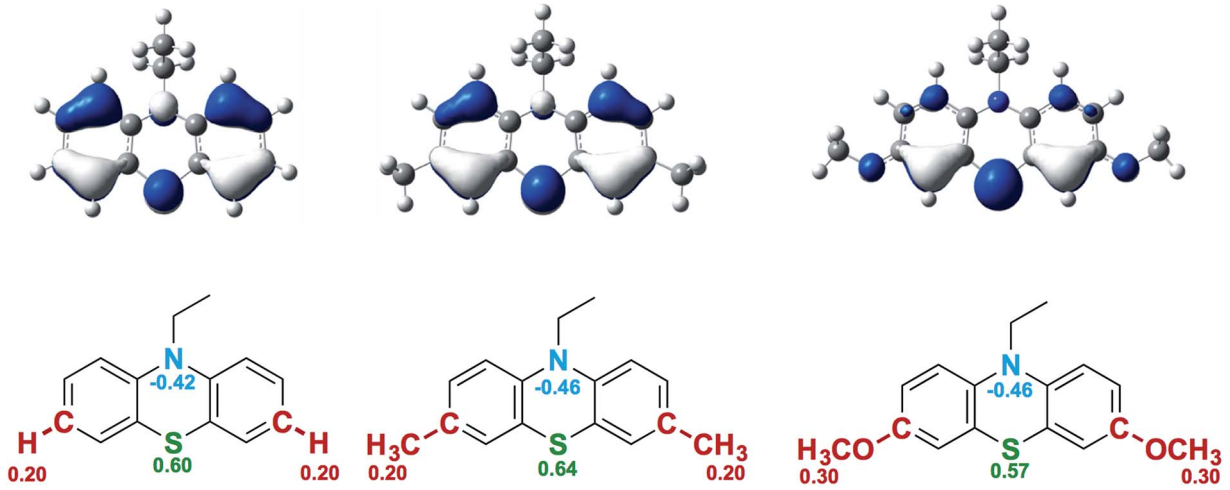

Fig. 4 Highest occupied molecular orbitals of the dications (top row) of EPT (left), DMeEPT (middle), and DMeOEPT (right), and select Mulliken charges for the dications of each of the molecules (bottom). All of the calculations were performed by DFT at the B3LYP/6-311G(d,p) level of theory.

electrode chamber of the bulk electrolysis cell. Note that *ca.* 80% of the theoretical capacity of the electrolyte solution was accessed because the cell must operate at *ca.* 25% of its limiting current, determined at 0% state of charge, in order to maintain the applied current. Cyclic voltammograms of the solution before and after cycling exhibit similar features (Fig. S17†), confirming that EPT is stable for the first electron transfer and validating the bulk electrolysis experiment. These results

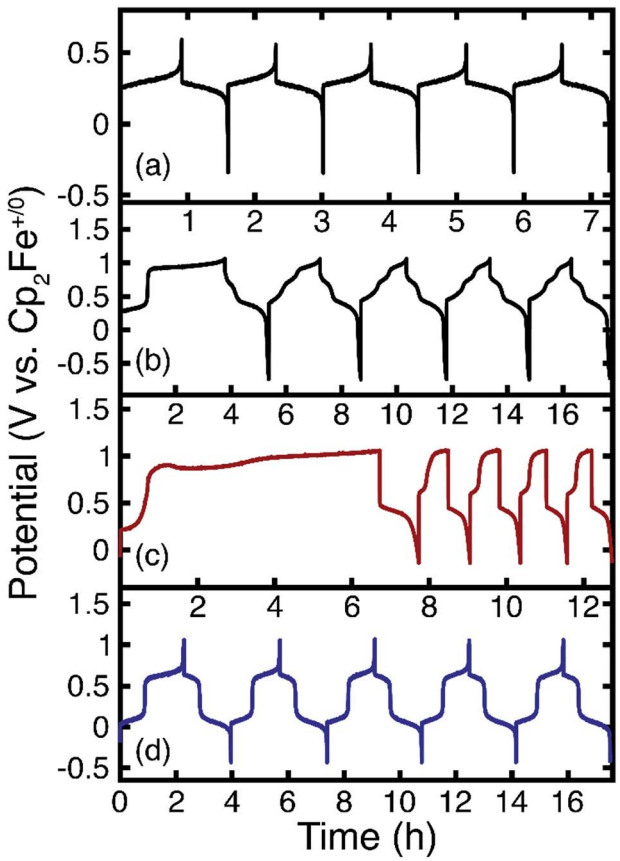

Fig. 5 Potential profiles for the first 5 cycles of bulk electrolysis charge/discharge experiments that access the first oxidation reaction of EPT (a). Potential profiles for the first 5 cycles of bulk electrolysis charge/discharge experiments that access the first and second oxidation reactions of EPT (b), DMeEPT (c), and DMeOEPT (d). All cycling was performed at 1 mM active material in 1 M LiTFSI in PC at a constant applied current of 0.804 mA.

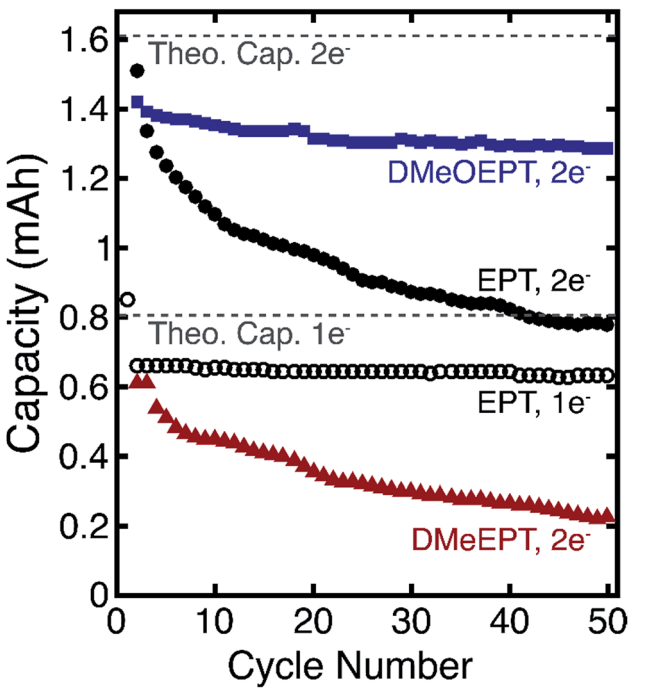

Fig. 6 Charging capacity *vs.* cycle number for bulk electrolysis charge/discharge experiments that access the first oxidation reaction of EPT (hollow, black circles), or both oxidation reactions for EPT (filled, black circles), DMeEPT (filled, red triangles), or DMeOEPT (filled, blue squares). All experiments were performed at 1 mM active species in 1 M LiTFSI in PC at a constant applied current of 0.804 mA. Note, in an attempt to represent the capacity more clearly, the first cycle for charging each material to two electrons is not shown because the accessed capacity for EPT and DMeEPT is much greater than the theoretical capacity.

demonstrate the stability of EPT in its neutral and radical-cation forms in the chosen electrochemical environment, consistent with previously reported studies on the stability of EPT.[43]

Bulk electrolysis was then extended to access the second oxidation of EPT using a fresh solution, which we expected would demonstrate the poor stability of EPT's dication. A cut-off potential of 1.05 V *vs.* $Cp_2Fe^{+/0}$ is sufficient to access the second oxidation event while minimizing electrolyte decomposition. After the first charge/discharge cycle, a new redox plateau appeared between the first and second oxidation potentials, suggesting the presence of a new redox species (Fig. 5b and S18†). This hypothesis is further supported by the initial charging half-cycle, which was nearly twice as long as expected (4 h rather than 2 h), suggesting an interplay between electrochemical oxidation and chemical reduction processes due to the instability of the dication form. All subsequent cycles exhibited three charging plateaus and two discharging plateaus. Over the course of the experiment, the cell capacity decreased by 50% (Fig. 6). The coulombic efficiency (Fig.S24†) ranged between 88 to 95% for the first 10 cycles, during which EPT decayed at a higher rate, accounting for roughly 65% of the total decay. After this initial period, the coulombic efficiency stabilized between 96 and 97%, and the EPT decay rate slowed. Cyclic voltammetry recorded before and after bulk electrolysis showed significant decay, as evidenced by the disappearance of well-defined redox waves (Fig. S19†). Early-stage decay was examined in a separate bulk electrolysis experiment in which cyclic voltammograms were recorded after the first and second charge/discharge cycles (Fig. S25†). Significant changes were observed over these first two cycles, indicating decomposition of the dication into one or more less stable electroactive species.

Satisfied that the radical cations of DMeEPT and DMeOEPT are stable, we next explored the degree to which the disparate *para* substituents stabilized the dications of these compounds. In bulk electrolysis experiments, the potential cut-off was set to 1.05 V *vs.* $Cp_2Fe^{+/0}$, allowing the second electron transfer event to be accessed while attempting to minimize electrolyte decomposition. The initial charging half cycle lasted three times longer than expected (6 h rather than 2 h), suggesting reductive decomposition of the DMeEPT dication into one or more unknown electroactive species, indicating the instability of the dication (Fig. 5c and S20†). The originally observed first-oxidation charging potential plateau was absent in subsequent cycles, and a new redox event around 0.6 V *vs.* $Cp_2Fe^{+/0}$ dominated further charging cycles (Fig. 6). Over the 50-cycle experiment, the capacity dropped to 13% of the theoretical value with the most-rapid decay occurring during the first 10 cycles (Fig. S24†). Cyclic voltammograms recorded before and after the 50-cycle experiment showed significant changes, including the appearance of a new ill-defined reduction wave around 0.4 V *vs.* $Cp^2Fe^{+/0}$, the same potential as the discharge plateau observed in bulk electrolysis (Fig. S21†). These observations indicate that methyl substituents *para* to nitrogen are insufficient to stabilize the dication in this environment.

Finally, we examined the stability of the DMeOEPT dication using bulk electrolysis experiments, again charging to 1.05 V *vs.* $Cp_2Fe^{+/0}$ (Fig. 5d and S22†). Here the cycling efficiency ranged from 98 to 100%, with an overall capacity retention of 93% after 50 cycles (Fig. 6 and S24†). Because the features in the original charge/discharge cycles remained consistent over the course of the 163 h experiment, we concluded that this fade is due to active-species crossover from the working-electrode chamber to the counter-electrode chamber rather than active-species decomposition. As before, we note that the theoretical capacity was not achieved (*ca.* 80%) in this experiment due to the applied current selected. The robustness of the dication is further supported by cyclic voltammograms recorded before and after cycling, which show nearly identical features. Only a slight decrease in peak height was observed, consistent with the capacity fade that occurs during cycling (Fig. S23†). From the results of these experiments, we concluded that the incorporation of methoxy groups *para* to the nitrogen atom effectively stabilized the DMeOEPT dication.

Experimental

Materials

Reagents and procedures used for synthesis are described in the ESI.†

X-ray crystallography

X-ray diffraction data were collected at 90.0(2) K on a Nonius kappaCCD diffractometer using MoK(α) X-rays. Raw data were integrated, scaled, merged, and corrected for Lorentz-polarization effects using the HKL-SMN package.[48] Corrections for absorption were applied using SADABS.[49] The structure was solved by direct methods,[50] and refinement was carried out against F^2 by weighted full-matrix least-squares.[51] Hydrogen atoms were found in difference maps but subsequently placed at calculated positions and refined using a riding model. Non-hydrogen atoms were refined with anisotropic displacement parameters. Atomic scattering factors were taken from the International Tables for Crystallography.[52]

Density functional theory calculations

All DFT calculations were performed using the Gaussian09 (Revision A.02b) software suite. Geometry optimizations of the neutral, radical-cation, and dication states were carried out with the B3LYP functional and 6-311G(d,p) basis set. Frequency analyses of all (fully relaxed) optimized geometries were performed to ensure that the geometries were energetic minima. Molecular orbitals were generated using an isovalue of 0.04.

Spectroelectrochemistry

Measurements on solutions containing 0.375 mM analyte (EPT, DMeEPT, or DMeOEPT) in 0.1 M LiTFSI in PC were performed using a spectroelectrochemical cell kit from Pine Research Instrumentation. The sample solution (1 mL) was placed in the quartz cuvette equipped with a Pt honeycomb electrode card, used as the working and counter electrodes, and a freshly anodized Ag/AgCl electrode used as the reference electrode. UV-vis spectra were obtained on an Agilent 8453 diode array spectrometer and electrochemical analysis was performed using a CH Instruments 650E potentiostat. First a UV-vis spectrum

and a cyclic voltammogram were recorded on the sample. Bulk electrolysis (with coulometry) was then performed for 1 min at 0.1 V increments from 0 to 2.0 V *vs.* Ag/AgCl (−0.18 to 1.82 V *vs.* $Cp_2Fe^{+/0}$) for EPT and DMeEPT, or from 0 to 1.5 V *vs.* Ag/AgCl (−0.18 to 1.32 V *vs.* $Cp_2Fe^{+/0}$) for DMeOEPT, and then back to 0 V *vs.* Ag/AgCl for all, followed by a UV-vis measurement at each of those potentials. The chosen potential window was obtained from the cyclic voltammetry measurement.

Electrochemical analysis

All electrochemical experiments for molecules evaluated in this study were performed in 1 M LiTFSI in PC. This solvent was chosen because of its wide electrochemical stability window, low volatility, moderate ionic conductivity, and compatibility with lithium salts (for a background scan, Fig. S14†). Cyclic voltammetry (CV) was performed to determine the chemical and electrochemical reversibility of each oxidation event and the diffusion coefficients of the neutral and radical-cation species. All CV experiments were performed at 1 mM with 100% IR correction. The resistance measured for each experiment was *ca.* 200 Ω, which leads to a correction of less than 0.5 mV for the largest measured currents.

All electrochemical measurements were performed in an argon-filled glovebox (MBraun Labmaster) with water <5 ppm and oxygen <1 ppm at 29 °C (ambient box temperature) using a VSP-300 potentiostat (Bio-Logic). All CV experiments were performed in a three-electrode cell with a 3 mm diameter glassy carbon disc working electrode (CH Instruments, Inc.), a gold coil counter electrode (CH Instruments, Inc.), and a fritted Li foil reference (Alfa Aesar). Before each measurement, the glassy carbon electrode was polished on a MicroCloth pad with 0.05 μm alumina powder (Buehler Ltd.). The electrode was then rinsed with deionized water (Millipore) and wiped with lens paper (VWR). To reference to $Cp_2Fe^{+/0}$, before each electrochemical measurement, an additional CV was performed on an electrolyte solution containing 5 mM ferrocene; the adjustment in potential of the ferrocene redox couple was applied to electrolyte solutions containing EPT, DMeEPT, and DMeOEPT to calibrate potentials to $Cp_2Fe^{+/0}$ at 0 V, similar to previous examples.[53] Diffusion coefficients for each of the charged and uncharged species were estimated using the Randles–Sevcik equation (Fig. S15†).

$$i_p = 0.4463nFAC\left(\frac{n\mathrm{FD}}{RT}\nu\right)^{0.5}$$

In the Randles–Sevcik equation i_p is the peak current (A), n is the number of electrons transferred (here, $n = 1$), F is the Faraday constant (96 485 C (mol e^-)$^{-1}$), A is the electrode area (0.0707 cm^2), C is the bulk concentration (0.001 M), R is the universal gas constant (8.314 J mol^{-1} K^{-1}), T is the temperature in Kelvin (302.15 K), D is the diffusion coefficient (cm^2 s^{-1}), and ν is the scan rate (V s^{-1}). The scan rates used to estimate the diffusion coefficients were 20, 30, 40, 50, 60, and 100 mV s^{-1}.

Bulk electrolysis

Extended-cycling (50-cycle) experiments were performed in a commercially available bulk electrolysis cell from BASi (MF-1056).[14] All long-term cycling experiments used 30 mL of electrolyte solution with 1 mM active species and were stirred at 1400 rpm. The working electrode, counter electrode, and reference electrode were reticulated vitreous carbon (BASi), lithium foil (Alfa Aesar), and fritted lithium foil (Alfa Aesar), respectively. The current for the galvanostatic cycling was set to 0.804 mA, such that the theoretical charging and discharging times were 1 h per electron transfer, based on the concentration and volume of the active material. This rate was selected to enable reasonable experimental runtimes, minimize species crossover, and facilitate high accessed capacity. Each solution was charged and discharged until a predetermined potential cut-off was reached, which was set to completely encompass the redox event. For the two-cycle experiment, a previously reported H-cell with a P5 ceramic frit (Adams & Chittenden Scientific Glass) was used starting with 3.5 mL of electrolyte solution with 5 mM active species on each side of the frit.[21,43] Reticulated vitreous carbon (45 ppi, ERG Aerospace Corp.) acted as both the working and counter electrodes, while fritted lithium foil (Alfa Aesar) was used as the reference electrode. Again, galvanostatic cycling was used with potential cut-offs set to completely charge and discharge the working solution. The current for the galvanostatic cycling was set to 0.469 mA, such that the theoretical charging and discharging times were 1 h per electron transfer, based on the concentration and volume of the active material. This rate was selected to enable reasonable experimental runtimes, minimize species crossover, and facilitate high accessed capacity. Each solution was charged and discharged until a predetermined potential cut-off was reached, which was set to completely encompass the redox event.

Conclusions

Compared to the unstable EPT dication, incorporating delocalizing, electron-donating methoxy groups at the positions *para* to nitrogen is more effective at stabilization than the electron-donating (but not delocalizing) methyl groups at the same positions. While the molecular weight of the new compound, DMeOEPT, is 26% larger than the parent compound, EPT, the stabilization of a second oxidation increases the overall molecular gravimetric capacity by 58%, leading to a charge storage capacity of 187 Ah kg^{-1}. This work provides an example of the successful design of a stable two-electron-donating organic species using simple modifications that extend the delocalization of charge in this small molecule. While the solubility of the species investigated here is too low for direct application in flow batteries, future efforts will focus on incorporating a more soluble version of DMeOEPT into nonaqueous flow cells. The use of soluble two-electron-transfer molecules with disparate redox events will introduce new challenges in cell polarization and battery efficiency that could offset some of the advantages associated with multi-electron transfer in RFBs. Understanding these cell-level tradeoffs will allow for the identification of design principles to improve molecular engineering efforts. More broadly, the experimental approach used in this work can be applied to advance the design of new redox-

active organic molecules for use in emerging electrochemical energy storage systems.

Conflicts of interest

There are no conflicts to declare.

Acknowledgements

Molecular synthesis and characterization studies were supported by the National Science Foundation (NSF), Division of Chemistry under Award Number CHE-1300653 and through the Experimental Program to Stimulate Competitive Research (EPSCoR), Award Number 1355438. Electrochemical studies were supported as part of the Joint Center for Energy Storage Research (JCESR), an Energy Innovation Hub funded by the U.S. Department of Energy, Office of Science, Basic Energy Sciences. SAO and CR thank the University of Kentucky for start-up funds. JDM acknowledges additional financial support from the NSF Graduate Research Fellowship Program (DGE 1256260). CFE thanks the ACS Division of Organic Chemistry for a SURF award.

Notes and references

1 P. Denholm, E. Ela, B. Kirby and M. Milligan, *The Role of Energy Storage with Renewable Electricity Generation*, National Renewable Energy Laboratory, Golden, Colorado, 2010.
2 I. Gyuk, *Grid Energy Storage*, US Department of Energy, Washington DC, 2013.
3 A. Z. Weber, M. M. Mench, J. P. Meyers, P. N. Ross, J. T. Gostick and Q. Liu, *J. Appl. Electrochem.*, 2011, **41**, 1137–1164.
4 B. R. Chalamala, T. Soundappan, G. R. Fisher, M. R. Anstey, V. V. Viswanathan and M. L. Perry, *Proc. IEEE*, 2014, **102**, 976–999.
5 R. M. Darling, K. G. Gallagher, J. A. Kowalski, S. Ha and F. R. Brushett, *Energy Environ. Sci.*, 2014, **7**, 3459–3477.
6 J. A. Kowalski, L. Su, J. D. Milshtein and F. R. Brushett, *Curr. Opin. Chem. Eng.*, 2016, **13**, 45–52.
7 J. Winsberg, T. Hagemann, T. Janoschka, M. D. Hager and U. S. Schubert, *Angew. Chem., Int. Ed.*, 2017, **56**, 686–711.
8 L. Eberson, *Adv. Phys. Org. Chem.*, 1982, **18**, 79–185.
9 I. Bertini, H. B. Gray, S. J. Lippard and J. S. Valentine, *Bioinorganic Chemistry*, University Science Books, Mill Valley, CA, 1994.
10 W. S. Jeon, H.-J. Kim, C. Lee and K. Kim, *Chem. Commun.*, 2002, 1828–1829.
11 Z. Li, S. Li, S. Liu, K. Huang, D. Fang, F. Wang and S. Peng, *Electrochem. Solid-State Lett.*, 2011, **14**, A171–A173.
12 F. R. Brushett, J. T. Vaughey and A. N. Jansen, *Adv. Energy Mater.*, 2012, **2**, 1390–1396.
13 X. Wei, W. Xu, M. Vijayakumar, L. Cosimbescu, T. Liu, V. Sprenkle and W. Wang, *Adv. Mater.*, 2014, **26**, 7649–7653.
14 J. Huang, L. Cheng, R. S. Assary, P. Wang, Z. Xue, A. K. Burrell, L. A. Curtiss and L. Zhang, *Adv. Energy Mater.*, 2015, **5**, 1401782.
15 A. P. Kaur, N. E. Holubowitch, S. Ergun, C. F. Elliott and S. A. Odom, *Energy Technol.*, 2015, **3**, 476–480.
16 T. Liu, X. Wei, Z. Nie, V. Sprenkle and W. Wang, *Adv. Energy Mater.*, 2016, **6**, 1501449.
17 X. Wei, W. Duan, J. Huang, L. Zhang, B. Li, D. Reed, W. Xu, V. Sprenkle and W. Wang, *ACS Energy Lett.*, 2016, **1**, 705–711.
18 R. A. Potash, J. R. McKone, S. Conte and H. D. Abruña, *J. Electrochem. Soc.*, 2016, **163**, A338–A344.
19 W. Wang, W. Xu, L. Cosimbescu, D. Choi, L. Li and Z. Yang, *Chem. Commun.*, 2012, **48**, 6669–6671.
20 X. Wei, W. Xu, J. Huang, L. Zhang, E. Walter, C. Lawrence, M. Vijayakumar, W. A. Henderson, T. Liu, L. Cosimbescu, B. Li, V. Sprenkle and W. Wang, *Angew. Chem., Int. Ed.*, 2015, **54**, 8684–8687.
21 C. S. Sevov, R. E. M. Brooner, E. Chénard, R. S. Assary, J. S. Moore, J. Rodríguez-López and M. S. Sanford, *J. Am. Chem. Soc.*, 2015, **137**, 14465–14472.
22 C. S. Sevov, D. P. Hickey, M. E. Cook, S. G. Robinson, S. Barnett, S. D. Minteer, M. S. Sigman and M. S. Sanford, *J. Am. Chem. Soc.*, 2017, **139**, 2924–2927.
23 C. S. Sevov, S. K. Samaroo and M. S. Sanford, *Adv. Energy Mater.*, 2017, **7**, 1602027.
24 A. Orita, M. G. Verde, M. Sakai and Y. S. Meng, *Nat. Commun.*, 2016, **7**, 13230.
25 B. Hu, C. DeBruler, Z. Rhodes and T. L. Liu, *J. Am. Chem. Soc.*, 2017, **139**, 1207–1214.
26 B. Huskinson, M. P. Marshak, C. Suh, S. Er, M. R. Gerhardt, C. J. Galvin, X. Chen, A. Aspuru-Guzik, R. G. Gordon and M. J. Aziz, *Nature*, 2014, **505**, 195–198.
27 K. Lin, Q. Chen, M. R. Gerhardt, L. Tong, S. B. Kim, L. Eisenach, A. W. Valle, D. Hardee, R. G. Gordon, M. J. Aziz and M. P. Marshak, *Science*, 2015, **349**, 1529–1532.
28 K. Lin, R. Gómez-Bombarelli, E. S. Beh, L. Tong, Q. Chen, A. Valle, A. Aspuru-Guzik, M. J. Aziz and R. G. Gordon, *Nat. Energy*, 2016, **1**, 16102.
29 J. Kopera and A. K. Armitage, *Br. J. Pharmacol.*, 1954, **9**, 392–401.
30 J. F. Casey, J. J. Lasky, C. J. Kleitt and L. E. Hollister, *Am. J. Psychiatry*, 1960, **117**, 97–105.
31 K. Taylor and H. Holtby, *J. Thorac. Cardiovasc. Surg.*, 2005, **130**, 566.
32 N. J. Treat, H. Sprafke, J. W. Kramer, P. G. Clark, B. E. Barton, J. Read de Alaniz, B. P. Fors and C. J. Hawker, *J. Am. Chem. Soc.*, 2014, **136**, 16096–16101.
33 E. H. Discekici, N. J. Treat, S. O. Poelma, K. M. Mattson, Z. M. Hudson, Y. Luo, C. J. Hawker and J. R. de Alaniz, *Chem. Commun.*, 2015, **51**, 11705–11708.
34 M. Gratzel, *Nature*, 2001, **409**, 575–576.
35 H.-J. Yen and G.-S. Liou, *J. Mater. Chem.*, 2010, **20**, 9886–9894.
36 D.-H. Hwang, S.-K. Kim, M.-J. Park, J.-H. Lee, B.-W. Koo, I.-N. Kang, S.-H. Kim and T. Zyung, *Chem. Mater.*, 2004, **16**, 1298–1303.
37 W. Wu, J. Yang, J. Hua, J. Tang, L. Zhang, Y. Long and H. Tian, *J. Mater. Chem.*, 2010, **20**, 1772–1779.

38 C. Buhrmester, L. Moshurchak, R. L. Wang and J. R. Dahn, *J. Electrochem. Soc.*, 2006, **153**, A288–A294.
39 L. M. Moshurchak, C. Buhrmester, R. L. Wang and J. R. Dahn, *Electrochim. Acta*, 2007, **52**, 3779–3784.
40 S. Ergun, C. F. Elliott, A. P. Kaur, S. R. Parkin and S. A. Odom, *Chem. Commun.*, 2014, **50**, 5339–5341.
41 A. P. Kaur, S. Ergun, C. F. Elliott and S. A. Odom, *J. Mater. Chem. A*, 2014, **2**, 18190–18193.
42 A. P. Kaur, M. D. Casselman, C. F. Elliott, S. R. Parkin, C. Risko and S. A. Odom, *J. Mater. Chem. A*, 2016, **4**, 5410–5414.
43 J. D. Milshtein, A. P. Kaur, M. D. Casselman, J. A. Kowalski, S. Modekrutti, P. Zhang, N. H. Attanayake, C. F. Elliott, S. R. Parkin, C. Risko, F. R. Brushett and S. A. Odom, *Energy Environ. Sci.*, 2016, **9**, 3531–3543.
44 S. A. Odom, S. Ergun, P. P. Poudel and S. R. Parkin, *Energy Environ. Sci.*, 2014, **7**, 760–767.
45 C. Hansch, A. Leo and R. W. Taft, *Chem. Rev.*, 1991, **91**, 165–195.
46 G. A. Olah and R. J. Spear, *J. Am. Chem. Soc.*, 1975, **97**, 1539–1546.
47 Z. Li, T. Bally, K. N. Houk and W. T. Borden, *J. Org. Chem.*, 2016, **81**, 9576–9584.
48 Z. Otwinowski and W. Minor, in *Methods in Enzymology*, Academic Press, 1997, vol. 276, pp. 307–326.
49 L. Krause, R. Herbst-Irmer, G. M. Sheldrick and D. Stalke, *J. Appl. Crystallogr.*, 2015, **48**, 3–10.
50 G. Sheldrick, *Acta Crystallogr., Sect. A: Found. Adv.*, 2015, **71**, 3–8.
51 G. Sheldrick, *Acta Crystallogr., Sect. C: Struct. Chem.*, 2015, **71**, 3–8.
52 *International Tables for Crystallography, vol C: Mathematical, Physical and Chemical Tables*, ed. E. Prince and T. R. Welberry, Kluwer Academic Publishers, Holland, 1992.
53 G. Gritzner and J. Kuta, *Pure Appl. Chem.*, 1984, **56**, 461–466.